Pentacene growth on the (111) surface of the 1/1 Au-Al-Tb approximant: Influence of surface geometry on adsorption

Sam Coates◉

Department of Materials Science and Technology, Tokyo University of Science, 6 Chome-3-1 Niijuku, Katsushika City, Tokyo 125-8585, Japan

Ronan McGrath and Hem Raj Sharma

Surface Science Research Centre and Department of Physics, University of Liverpool, Liverpool L69 3BX, United Kingdom

Ryuji Tamura◉

Department of Materials Science and Technology, Tokyo University of Science, 6 Chome-3-1 Niijuku, Katsushika City, Tokyo 125-8585, Japan

Molecular adsorption on both quasicrystalline and approximant substrates has produced a number of pseudo-morphic films, and has led to a deeper understanding of the chemistry of the surfaces of these materials. Here, the recently reported reconstructed (111) surface of the 1/1 Au-Al-Tb Tsai-type approximant has been used as a template for pentacene (Pn) adsorption, which is investigated using scanning tunneling microscopy. This surface provides unique varieties of adsorption sites compared to a normal metal surface. After room-temperature deposition, the Pn molecules are mobile yet exhibit a structure which indicates a bond with the Tb atoms of the surface, while reflecting the twofold symmetrical nature of the reported Au/Al row reconstruction. Postdeposition annealing shows a linear arrangement of molecules in a specific adsorption geometry, likely corresponding to the most favorable energetic configuration.

I. INTRODUCTION

The wide compositional variety in Tsai-type quasicrystals and approximants has led to the observation of a range of phase-specific and stoichiometric-specific properties [1–6], including a rich array of magnetic transitions [7–12]. The shared building block of these materials, the Tsai-type cluster, is a hierarchical polyhedral structure consisting of five atomic shells: a tetrahedron, dodecahedron, icosahedron, icosido-decahedron, and rhombic triacontahedron [13–15]. These polyhedra and their nested nature are indicated in Fig. 1(a) by the black arrows, where the first shell is gray, the second is yellow, the third is green, the fourth is blue, and the fifth is red. The exact structure determination of Tsai-type materials gives license for a deep understanding of their properties, and allows for informed analyses of their surfaces.

In general, the surfaces of quasicrystal approximants offer a diverse field of investigation, as their structural and chemical behavior can be dissimilar to their quasicrystalline analogs, despite their common building blocks (not exclusive to Tsai types). For instance, reconstructions (not seen in quasicrystals) and high surface corrugations indicate a potential for catalytic activity [16–18], while the periodicity of approximant surfaces offer different, yet novel, energetic landscapes for adsorbates [19–21].

We recently showed that the (111) surface of the antiferromagnetic 1/1 $Au_{70}Al_{16}Tb_{14}$ Tsai-type approximant forms a partial reconstruction [22]—the first reconstruction observed at a Tsai-type approximant surface [23,24]. Here, the Au/Al atoms create a row-type structure, while the Tb atoms

conform to the expected bulk truncation: small triangles in two 60°-related orientations and larger triangles in a singular orientation. A model of this surface structure is shown in Fig. 1(b) where the atoms of specific shells are colored according to Fig. 1(a), and the Tb triangles are outlined with black lines. This juxtaposition of twofold (Au/Al) and threefold (Tb) symmetry presents an intriguing playground for adsorption studies.

Here, we present the deposition of pentacene (Pn) molecules onto the (111) surface of the 1/1 Au-Al-Tb approximant. There have been many previous surface studies utilizing organic molecules such as pentacene and C_{60} on quasicrystal and approximant surfaces [19,25–31]. In such studies, establishing the molecular adsorption geometry typically reveals useful knowledge about the underlying surface structure and reactivity. The molecule acts as a chemical probe of the surface, while also yielding useful information on the role of intermolecular interactions in ordering processes on complex surfaces. Here, at low coverage the Pn molecules are relatively mobile but are shown to adsorb at specific Tb sites. The observed orientational anisotropy of the adsorbed molecules indicates that there are certain preferred sites. Postannealing of higher coverages reveals a linear Pn structure which appears related to the reconstructed Au/Al rows of the substrate.

II. METHODS

The (111) surface of a single crystal of 1/1 Au-Al-Tb was polished with successively finer grades of diamond paste
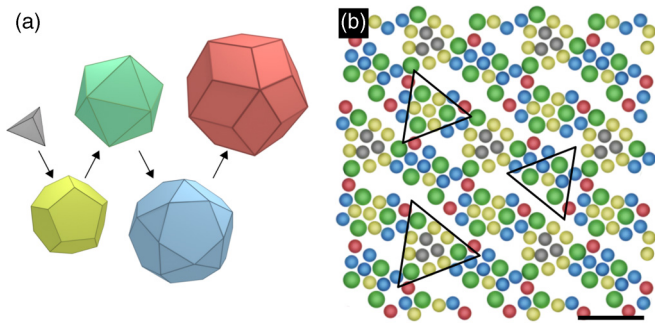
FIG. 1. (a) The hierarchical Tsai-cluster model. (b) Model of the (111) surface of the 1/1 Au-Al-Tb approximant. Green circles correspond to Tb atoms, and the remaining colors are a stoichiometric mix of Au/Al. Black triangles contain Tb triangles described in the main text. The scale bar is 1.5 nm.

(6–0.25 μm) before washing in methanol. The surface was then further cleaned with sputter-anneal cycles (30-min Ar$^+$ sputter, 2-h anneal at 730 K) under ultrahigh vacuum conditions. Substrate cleanliness was monitored with room-temperature scanning tunneling microscopy (STM), where STM bias is given with respect to the sample. Pn was dosed using a homemade evaporator. Due to the location of the evaporator, the molecules were deposited on the sample held at room temperature, before postdose annealing. The specifics of

the molecular annealing temperatures and times are discussed later.

III. RESULTS AND DISCUSSION

Figure 2(a) shows an STM image of approximately 0.3 monolayers (ML) of Pn on the Au-Al-Tb(111) surface. The structure of the surface is observed as corrugated rows, as previously reported under the bias conditions applied [22]. The coverage is estimated by removing the substrate contribution to the image area via a flooding algorithm [32]. In this case, 1 ML refers to complete areal coverage of the scan with molecules; the approximate number of molecules deposited was 0.11 per nm^2. The sample was held at room temperature during deposition, after which it was annealed at $\sim$370 K for 10 min. The Pn molecules appear to sparsely decorate a rhombohedral lattice, demonstrated by the inset autocorrelation function which was calculated considering the centers of the molecules as points. In the autocorrelation function, the rhombohedral lattice has the following (labeled) vectors: $a = 1.26 \pm 0.08$ nm, $b = 1.28 \pm 0.05$ nm.

Successive STM images of the same area indicate that Pn molecules diffuse at room temperature—both rotating and hopping across the surface. The mobility of the molecules is inferred in the streaklike tip artifacts in Fig. 2(a). However, we find relatively stable positions by analyzing the orientational anisotropy of the Pn molecules. Figure 2(b)
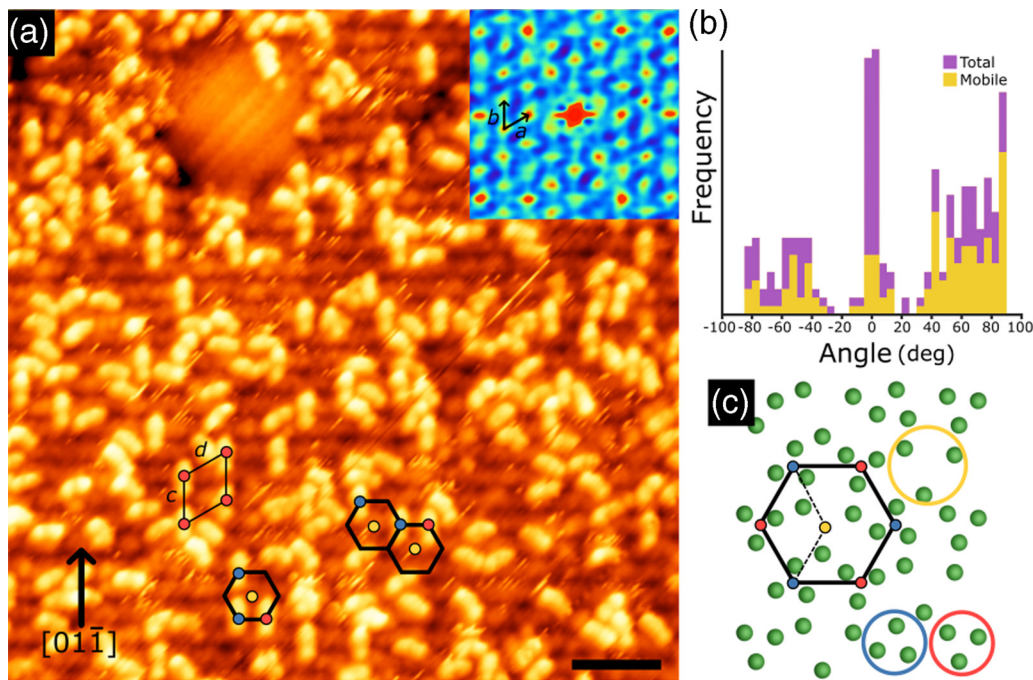
FIG. 2. (a) STM image ($V_b = -1900$ mV, $I_t = 300$ pA) of the Au-Al-Tb(111) surface after deposition of 0.3 ML of Pn. Highlighted by red and blue dots are molecules which are both oriented along the same direction yet occupy distinctly different adsorption sites. These molecules occupy a honeycomb lattice, as marked by a black hexagon. Yellow dots indicate vacant positions. A red dotted rhombus indicates the unit cell of the red dot distribution. The inset is an autocorrelation function of the molecule centers, with unit cell vectors marked. The [01$\bar{1}$] direction is indicated by a black arrow. The scale bar is 5 nm. (b) A histogram of molecular orientations. Orange bars represent the total number of orientations, and yellow bars represent the ratio of molecules which are observed diffusing. Values are shifted by 7° for clarity (explained in the main text). (c) A model of the Tb atoms at the surface. Blue and red circles indicate small Tb triangles which form a hexagonal unit cell, as marked in black. A larger yellow circle indicates a subsurface triangle. Small red, blue, and yellow dots sit at the center of these triangles, replicating the motif in (a). A dashed line indicates the cell formed by red, blue, and yellow triangles.
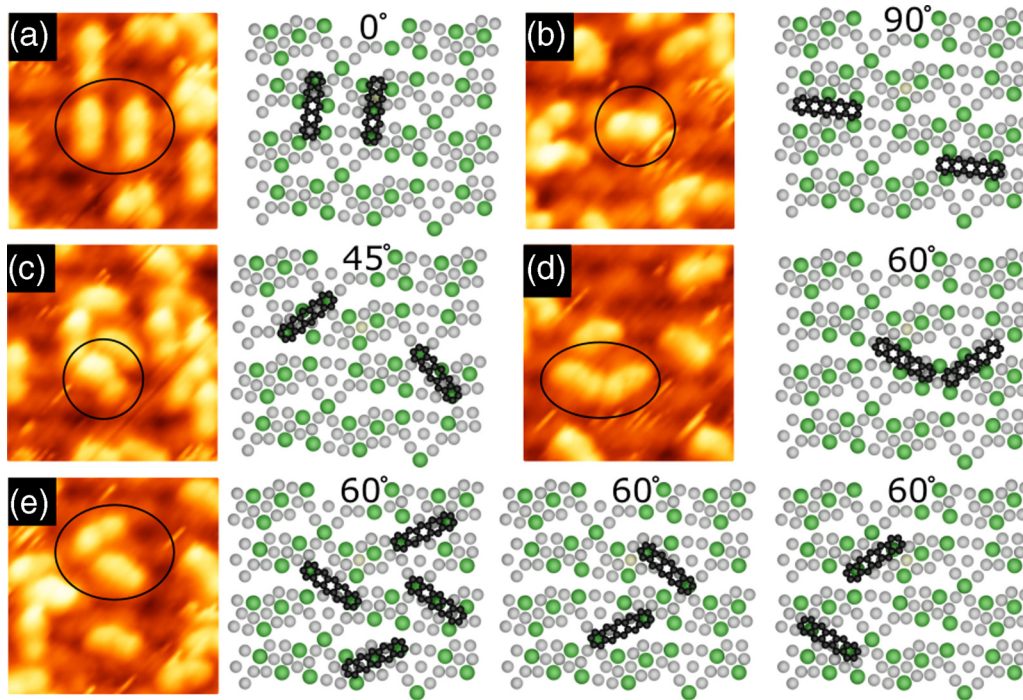
FIG. 3. (a)–(e) Enlarged STM images from Fig. 2(a) and model representations of Pn adsorption sites for a range of Pn orientations. The relevant molecules are circled in black. In each case, the Pn molecule is either adsorbing directly on-top multiple Tb atoms [e.g., (c), (e) middle and right], pinned by closely separated Tb atoms [(b), (d)] or a mixture of both (remaining).

shows a histogram of the molecular orientations. The angles are measured with respect to the absolute vertical direction of the image, [01$\bar{1}$], which is marked with an arrow in Fig. 2(a). The angles are shifted by $\sim -7°$ for clarity, which is explained later. The purple bars represent the total distribution as calculated over ten successive images, while the yellow bars show the orientations of molecules which are observed diffusing. It is clear, by both the total count and the ratio of diffusing to stationary molecules, that the most stable adsorption sites are those producing Pn orientations roughly perpendicular to the row direction of the substrate (0°). Conversely, the perpendicular twofold orientation (90°) is relatively unstable, a large proportion of these molecules are diffusing.

By marking all molecules aligned along the [01$\bar{1}$] direction, we find that they occupy two triangular sublattices which, together, form a honeycomb structure. Examples are indicated in Fig. 2(a) with red/blue circles and black hexagons. A fully occupied unit cell of the red distribution is also marked, with $c = 2.23 \pm 0.06$ nm, $d = 2.35 \pm 0.07$ nm, i.e., twice the size of the lattice measured from the inset autocorrelation function. Notably, the third triangular lattice—whose inclusion into the red/blue honeycomb structure would recreate the lattice measured in the autocorrelation function—is unoccupied across the surface. Examples of these sites are highlighted by yellow circles at the center of the hexagons.

The sublattice/honeycomb structure of the red/blue sites matches the distribution of small Tb triangles at the surface. This relationship is indicated in Fig. 2(c) which shows a section of the model Tb atoms at the surface [22]. Two small triangles at the bottom are enclosed by blue and red circles,

which are each distributed on rhombohedral lattices of $c = d = 2.09$ nm across the surface. These triangles are canted $\sim 7°$ with respect to the [01$\bar{1}$] direction and can also be linked by a black hexagon, with the centers of the triangles marked with either red or blue dots. The center of the hexagon shows a yellow dot at the center of a larger, subsurface Tb triangle and a dashed lined indicates the cell formed between red, blue, and yellow dots.

We can therefore speculate on potential adsorption sites for all orientations across the surface considering the match between the underlying Tb structure and the [01$\bar{1}$]-oriented molecule distribution. Figure 3 shows a collection of enlarged images from Fig. 2(a) and model representations of Pn adsorption sites, dependent on orientation. Only orientations with significant peaks in Fig. 2(b) are considered: 0°, 45°, 60°, and 90° (including any mirror equivalents), i.e., those commensurate with twofold row (0°, 45°, 90°) and threefold triangular (0°, 60°) symmetry. As previously mentioned, the Pn molecules are typically canted from these absolute orientations, roughly by the same small angle as the Tb triangles (7° with respect to the absolute vertical direction). For simplicity, however, we label the figures with respect to the shifted histogram values.

From a geometric standpoint, each adsorption site involves Tb atoms interacting with the ends of the Pn molecule through either (a) an on-top acene ring–Tb atom interaction (e.g., 45°), (b) mirror-symmetric pinning between two Tb atoms, presumably mediated by the H atoms on the acene ring (e.g., 90°), or (c) a mixture of both. This observation is consistent with previous work of Pn adsorption on Tsai-type surfaces, where the molecules preferentially adsorb at the sparsely distributed rare-earth atom positions [27,30]. Similarly, the relative chem-
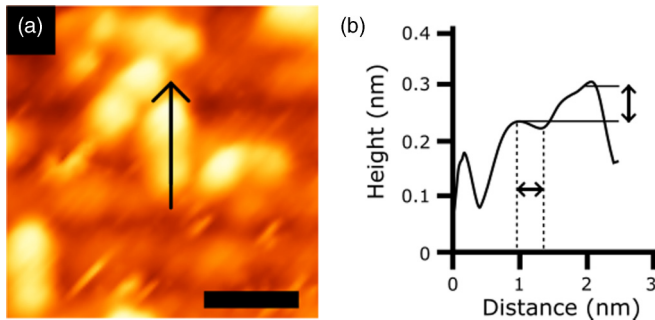
FIG. 4. (a) STM image showing molecules with bright and dim lobes. An arrow indicates the direction of the line profile in (b). The scale bar is 2 nm. (b) Line profile from (a). Horizontal dashed lines indicate the distance between the dim lobe and the molecular center. Solid horizontal lines mark the apparent lobe height difference.

ical order of the Tb positions compared to the Au/Al atoms likely makes a more consistent "choice" for the molecules.

Electronically, the signal observed by STM for the molecules generally show a double-lobe structure consistent with relatively poor molecular resolution of Pn on metal surfaces [33–35]. On a local level, the Pn molecules often exhibit a difference in contrast between the two lobes, demonstrated by the examples in Fig. 4(a). With STM, these differences can be considered as either a change in height, electronic contribution, or both. Analysis of the substrate under the brighter lobes indicates no change in morphology to cause a significant height modulation—despite the row structure of the reconstruction. Likewise, the length of the molecules in all orientations is equal, indicating a planar adsorption scheme independent of orientation. Therefore, we suggest that this effect is electronic.

To illustrate this, Fig. 4(b) shows a line profile taken in the direction of the arrow marked in Fig. 4(a). The profile indicates the apparent change in height along a $0°$ oriented molecule, marked by the two horizontal black lines, which on average across the image is measured as 0.05 ± 0.02 nm (for $0°$ molecules). For context, the apparent average height of all molecules above the substrate is ~ 0.8–1.2 nm, consistent with Pn on metal surfaces [33]. Furthermore, it appears that the brighter lobe is smeared towards the dimmer lobe, shifting the center (or dip) of the molecular signal. This is demonstrated in Fig. 4(b) by the dashed vertical lines, as measured from the dimmer lobe to the "lowest" point in the molecule. Across the image for the $0°$ molecules, this distance is measured as 0.37 ± 0.06 nm, indicating an anisotropy in the electronic signal as the expected center should be half of the electronic Pn length (~ 0.5 nm [33]). Measuring the height change and lobe center over all orientations shows that only the $0°$ molecules have one lobe which is consistently brighter and smeared towards the center (i.e., the bright-lobe effect appears to cancel out over the other orientations).

Referring back to Fig. 3, we see for the $0°$ molecules that the "top" poles of both molecules lie in close proximity to three Tb atoms, while their "bottom" poles are near one to two. Meanwhile, the other orientations have (on average) equal local environments through their mirror-symmetric pairs. Therefore, we suggest that bright-lobe effect is caused

by the higher density of Tb atoms at the $0°$ sites, indicating a higher flow of electrons into these Pn poles. Indeed, the anisotropic smearing of the brighter lobes can be explained by the Tb triangles at the $0°$ sites in Fig. 3(a) covering an area approximately equal to three acene rings out of five. This would shift the apparent "center" of the molecule to the 2:3 ring junction or ~ 0.4 nm from the bottom pole—an excellent match with the measured apparent centers.

We can speculate on the relative stability of the $0°$ site by directly comparing it to the other orientations in Figs. 3(a)–3(e). For the $90°$ site, both adsorption sites are commensurate with the row structure of the Au/Al atoms, i.e., adsorbing along the troughs between adjacent rows. However, Fig. 3(b) shows that the $90°$ positions are reliant on the Tb-pinning sites only. This suggests that the on-top acene ring interaction is a key to stability. Figures 3(c) and 3(e), orientations $45°$ and $60°$, all show some degree of on-top acene ring–Tb interaction, however, they are also incommensurate with the twofold symmetry of the Au/Al row structure, i.e., not in registry with the symmetric directions of the underlying surface. Figure 3(d), $60°$, is a unique case, only appearing once within Fig. 2(a). Indeed, it neither features an on-top interaction, nor symmetry sharing with the row structure.

Figure 5(a) shows an STM image after further deposition of Pn molecules, approximately 0.7 ML, which was not postannealed. The inset shows two autocorrelation functions with the same scale: The left is a function calculated from the center positions of the molecules while disregarding their orientation, while the right considers both. It is clear that while the film is structurally ordered, the orientational structure of the molecules is relatively disordered. Figure 5(b) shows an STM scan after postannealing the sample to 600 K. The left inset of Fig. 5(b) shows an autocorrelation function of the molecular distribution independent of orientation, while the right inset considers the orientation. A clear enhancement of a rectangularlike structure is observed. Likewise, the coverage is reduced, ~ 0.5 ML, where Pn molecules which are not strongly bonded to the surface are presumed to desorb in the annealing process.

Figure 6 shows the histogram of molecular orientations after the annealing process, taken over a similar-sized area as Fig. 2(b) (~ 35 nm $\times$ 35 nm), which reflects a clearer orthogonal preference in comparison to Fig. 2(b). Now, the majority of molecules are aligned along the $[01\bar{1}]$ direction ($\sim 56\%$), with several rows of molecules observed, marked by an arrow in Fig. 5(b). A minority of the Pn molecules are oriented $90°$ ($\sim 27\%$), while the remaining $\sim 11\%$ are either $60°$ or $45°$. In comparison, the ratio of orientations in Fig. 2(b) is $\sim 21\%$ for $0°$, $\sim 12\%$ for $90°$, with the remaining molecules orientated between $45°$ and $60°$.

Analysis of the Pn row structures indicate that the postdeposition annealing promotes new adsorption sites. Figure 5(c) shows an enlarged section of Fig. 5(b), where the Pn molecules are now decorated with colored arrows or bars. The colors represent the positions of the Tb triangles at the surface indicated in Fig. 2(c), while the direction of the arrows indicates their relationship to these sites, explained in Fig. 5(d). Here, the original $0°$ sites discussed in Fig. 2(a)
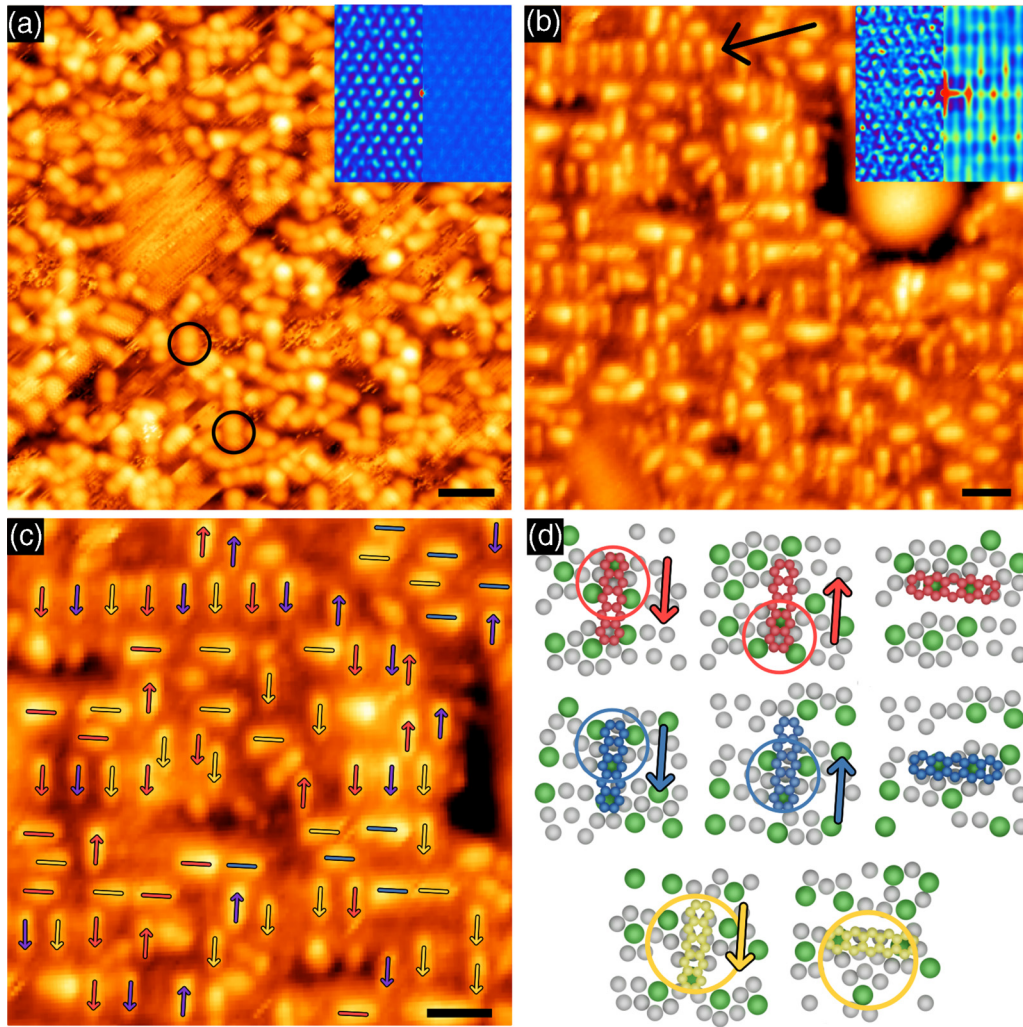
FIG. 5. (a) STM image ($V_b = -1800$ mV, $I_t = 300$ pA) of 0.7 ML of Pn with no postannealing. Examples of molecules aligned along the vertical direction are marked by black circles. Inset (left): The autocorrelation function of the molecular centres. Inset (right): The autocorrelation function including the molecular orientations. The scale bar is 3 nm. (b) STM image ($V_b = -1800$ mV, $I_t = 300$ pA) of the same dose of Pn, after annealing to 600 K. The molecules show a clear preference for the vertical direction. A row of Pn molecules is highlighted by an arrow. The scale bar is 3 nm. (c) Individual Pn molecules are labeled with colored arrows with respect to their adsorption sites. Red, blue, and yellow correspond to the Tb triangles in Fig. 2(c). The direction of the arrow corresponds to the adsorption site geometry. The scale bar is 2 nm. (d) Model representation of the adsorption sites. The up and down arrows correspond to the positions of the molecules with respect to the Tb triangles. The colored circles indicate the Tb triangles as in Fig. 2(c).

correspond to the red or blue down-pointing arrows. The up arrows represent molecules adsorbed at the same Tb triangles which are now slightly shifted vertically with respect to the underlying substrate: Red or blue circles indicate the respective Tb triangles at the surface. Yellow arrow sites involve the larger subsurface Tb triangle, and only appear in one "orientation," i.e., a down arrow. This is likely due to the large Tb triangle only appearing in one orientation at the surface, unlike the small triangles.

Horizontal (90°) Pn molecules are represented by colored bars, and now appear to adsorb directly on top of the Au/Al rows (interpreted by the relative positions of the other molecules), unlike those in Fig. 3(b). It is likely that the additional thermal energy allows the 90°-oriented molecules to escape the hollows between adjacent bright rows. For all of the horizontal molecules, two rings of the Pn molecule sit on

top of Tb atoms, either towards the center (red/blue) or at the ends of the Pn (yellow).

The bright-lobe and smeared center effects are still observed after the postannealed treatment promotes new sites. The down-pointing molecules (again, which represent the majority) exhibit a brighter lobe at the "top" pole with an apparent height change of 0.03 ± 0.01 nm and a center "dip" at 0.3 ± 0.1 nm as measured from the dimmer lobe. This is in agreement with the previous values, and the higher concentration of Tb atoms at the top position. The up-pointing molecules show brighter lobes at the top poles (0.02 ± 0.02 nm), despite a higher concentration of Tb atoms at their bottom poles, although the uncertainty on this value suggests inconsistency. Likewise, their apparent center is now measured as 0.48 ± 0.06 nm from the dimmer pole. A similar effect is observed for the horizontal
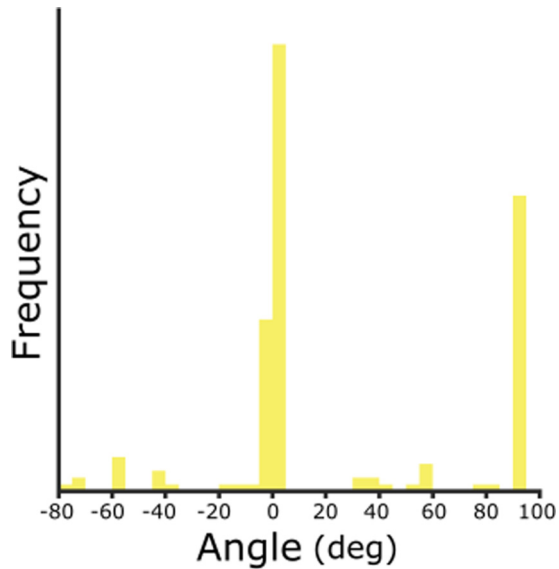
FIG. 6. Histogram of molecular orientation after postdeposition annealing to 600 K. Compared to Fig. 2(b), the range of molecular orientations has been reduced so that only vertical or horizontal molecules are observed.

molecules. A possible explanation for these small changes is the role of Au/Al chemical disorder in the now-promoted sites affecting the electronic state of the molecule. Like-wise, the electronic landscape of the interface can be affected by molecular adsorption [36], so that the majority down-pointed molecules indirectly and subtly affect the remaining minority.

IV. CONCLUSIONS

We have shown that Pn molecules deposited onto the (111) surface of the 1/1 Au-Al-Tb approximant form a rotation-ally aligned film after annealing to 370 K, influenced by the underlying twofold symmetry of the Au/Al row structure. Stable sites were found to involve rare-earth atoms either by an on-top Tb–acene ring interaction, or by a pinning of the ring between two closely separated Tb atoms. Analysis of the apparent height difference and center points of the $0°$ molecule lobes indicated a greater electronic contribution at Tb-dense sites. Further deposition without annealing showed that the Pn molecules form a structurally ordered film with poor rotational order. Additional annealing to 600 K decreased the Pn coverage and promoted diffusion of the molecules, leading to a more strongly ordered film.

[1] K. Deguchi, M. Nakayama, S. Matsukawa, K. Imura, K. Tanaka, T. Ishimasa, and N. K. Sato, Crystal structure of superconducting 1/1 cubic Au-Ge-Yb approximant with Tsai-type cluster, J. Phys. Soc. Jpn. **84**, 015002 (2015).

[2] K. Deguchi, M. Nakayama, S. Matsukawa, K. Imura, K. Tanaka, T. Ishimasa, and N. K. Sato, Superconductivity of Au-Ge-Yb approximants with Tsai-type clusters, J. Phys. Soc. Jpn. **84**, 023705 (2015).

[3] T. Watanuki, S. Kashimoto, D. Kawana, T. Yamazaki, A. Machida, Y. Tanaka, and J. S, Taku, Intermediate-valence icosahedral Au-Al-Yb quasicrystal, Phys. Rev. B **86**, 094201 (2012).

[4] K. Deguchi, S. Matsukawa, N. K. Sato, T. Hattori, K. Ishida, H. Takakura, and T. Ishimasa, Quantum critical state in a magnetic quasicrystal, Nat. Mater. **11**, 1013 (2012).

[5] S. Jazbec, S. Vrtnik, Z. Jagličić, S. Kashimoto, J. Ivkov, P. Popčević, A. Smontara, H. J. Kim, J. G. Kim, and J. Dolinšek, Electronic density of states and metastability of icosahedral Au-Al-Yb quasicrystal, J. Alloys Compd. **586**, 343 (2014).

[6] K. Kamiya, T. Takeuchi, N. Kabeya, N. Wada, T. Ishimasa, A. Ochiai, K. Deguchi, K. Imura, and N. K. Sato, Discovery of superconductivity in quasicrystal, Nat. Commun. **9**, 1 (2018).

[7] A. Ishikawa, T. Hiroto, K. Tokiwa, T. Fujii, and R. Tamura, Composition-driven spin glass to ferromagnetic transition in the quasicrystal approximant Au-Al-Gd, Phys. Rev. B **93**, 024416 (2016).

[8] A. Ishikawa, T. Fujii, T. Takeuchi, T. Yamada, Y. Matsushita, and R. Tamura, Antiferromagnetic order is possible in ternary quasicrystal approximants, Phys. Rev. B **98**, 220403(R) (2018).

[9] S. Yoshida, S Suzuki, T. Yamada, T. Fujii, A. Ishikawa, and R. Tamura, Antiferromagnetic order survives in the higher-order quasicrystal approximant, Phys. Rev. B **100**, 180409(R) (2019).

[10] H. Miyazaki, T. Sugimoto, K. Morita, and T. Tohyama. Magnetic orders induced by RKKY interaction in Tsai-type quasicrystalline approximant Au-Al-Gd, Phys. Rev. Mater. **4**, 024417 (2020).

[11] T. J. Sato, A. Ishikawa, A. Sakurai, M. Hattori, M. Avdeev, and R. Tamura. Whirling spin order in the quasicrystal approximant $Au_{72}Al_{14}Tb_{14}$, Phys. Rev. B **100**, 054417 (2019).

[12] R. Tamura, Y. Muro, T. Hiroto, K. Nishimoto, and T. Takabatake. Long-range magnetic order in the quasicrystalline approximant Cd_6Tb, Phys. Rev. B **82**, 220201(R) (2010).

[13] H. Takakura, C. P. Gómez, A. Yamamoto, M. de Boissieu, and A. P. Tsai, Atomic structure of the binary icosahedral Yb-Cd quasicrystal, Nat. Mater. **6**, 58 (2007).

[14] A. P. Tsai, J. Q. Guo, E. Abe, H. Takakura, and T. J. Sato, Alloys: A stable binary quasicrystal, Nature **408**, 537 (2000).

[15] A. P. Tsai, Icosahedral clusters, icosahedral order and stability of quasicrystals'a view of metallurgy, Sci. Technol. Adv. Mater. **9**, 013008 (2008).

[16] J. K. Parle, A. Beni, V. R. Dhanak, J. A. Smerdon, P. Schmutz, M. Wardé, M-G. Barthés-Labrousse, B. Bauer, P. Gille, and H. R. Sharma, STM and XPS investigation of the oxidation of the $Al_4(Cr,Fe)$ quasicrystal approximant, Appl. Surf. Sci. **283**, 276 (2013).

[17] J. Ledieu, É. Gaudry, L. N. S. Loli, S. A. Villaseca, M.-C. De Weerd, M. Hahne, P. Gille, Y. Grin, J.-M. Dubois, and

V. Fournée, Structural Investigation of the (010) Surface of the $Al_{13}Fe_4$ Catalyst, Phys. Rev. Lett. **110**, 076102 (2013).

[18] C. Chatelier, Y. Garreau, A. Vlad, J. Ledieu, A. Resta, V. Fournée, M-C. De Weerd, A. Coati, and É. Gaudry, Pseudo-2-fold surface of the $Al_{13}Co_4$ catalyst: Structure, stability, and hydrogen adsorption, ACS Appl. Mater. Interfaces **12**, 39787 (2020).

[19] J. Ledieu, É. Gaudry, K. Pussi, T. Jarrin, P. Scheid, P. Gille, and V. Fournée, Reconstruction of the $Al_{13}Ru_4$ (010) approximant surface leading to anisotropic molecular adsorption, J. Phys. Chem. C **121**, 22067 (2017).

[20] V. Fournée, A. R. Ross, T. A. Lograsso, J. W. Evans, and P. A. Thiel, Growth of Ag thin films on complex surfaces of quasicrystals and approximant phases, Surf. Sci. **537**, 5 (2003).

[21] V. Fournée, J. A. Barrow, M. Shimoda, A. R. Ross, T. A. Lograsso, P. A. Thiel, and A. P. Tsai, Palladium clusters formed on the complex pseudo-10-fold surface of the ξ'-$Al_{77.5}Pd_{19}Mn_{3.5}$ approximant crystal, Surf. Sci. **541**, 147 (2003).

[22] S. Coates, K. Nozawa, M. Fukami, K. Inagaki, M. Shimoda, R. McGrath, H. R. Sharma, and R. Tamura, Atomic structure of the (111) surface of the antiferromagnetic 1/1 Au-Al-Tb approximant, Phys. Rev. B **102**, 235419 (2020).

[23] S. Hars, H. Sharma, J. Smerdon, T. Yadav, R. Tamura, M. Shimoda, and R. McGrath, The structure of the (100) surface of Ag-In-Gd 1/1 approximant, Acta Phys. Pol., A **126**, 479 (2014).

[24] S. S. Hars, H. R. Sharma, J. A. Smerdon, T. P. Yadav, A. Al-Mahboob, J. Ledieu, V. Fournée, R. Tamura, and R. McGrath, Surface structure of the Ag-In-(rare earth) complex intermetallics, Phys. Rev. B **93**, 205428 (2016).

[25] V. Fournée, É. Gaudry, J. Ledieu, M.-C. De Weerd, D. Wu, and T. Lograsso, Self-organized molecular films with long-range quasiperiodic order, ACS Nano **8**, 3646 (2014).

[26] J. Ledieu, É. Gaudry, V. Fournée, J. A. Smerdon, and R. D. Diehl Fullerene adsorption on intermetallic compounds of increasing structural complexity. Zeitschrift für Kristallographie-Crystalline Materials, **232**, 629-645 (2017).

[27] J. A. Smerdon, K. M. Young, M. Lowe, S. S. Hars, T. P. Yadav, D. Hesp, V. R. Dhanak, A. P. Tsai, H. R. Sharma, and R. McGrath, Templated quasicrystalline molecular ordering, Nano Lett. **14**, 1184 (2014).

[28] É. Gaudry, J. Ledieu, and V. Fournée, The role of three-dimensional bulk clusters in determining surface morphologies of intermetallic compounds: Quasicrystals to clathrates, J. Chem. Phys. **154**, 124706 (2021).

[29] N. Kalashnyk, J. Ledieu, É. Gaudry, C. Cui, A. P. Tsai, and V. Fournée, Building 2D quasicrystals from 5-fold symmetric corannulene molecules, Nano Res. **11**, 2129 (2018).

[30] A. Alofi, D. Burnie, S. Coates, R. McGrath, and H. R. Sharma, Adsorption of pentacene on the 2-fold surface of the icosahedral Ag-In-Yb quasicrystal, Mater. Trans. **62**, 312 (2021).

[31] S. Coates, J. A. Smerdon, R. McGrath, and H. R. Sharma, A molecular overlayer with the Fibonacci square grid structure, Nat. Commun. **9** (2018).

[32] I. Horcas, R. Fernández, J. M. Gomez-Rodriguez, J. Colchero, J. W. J. Gómez-Herrero, and A. M. Baro, WSXM: A software for scanning probe microscopy and a tool for nanotechnology, Rev. Sci. Instrum. **78**, 013705 (2007).

[33] J. Lagoute, K. Kanisawa, and S. N. Fölsch, Manipulation and adsorption-site mapping of single pentacene molecules on Cu (111), Phys. Rev. B **70**, 245415 (2004).

[34] C. B. France, P. G. Schroeder, J. C. Forsythe, and B. A. Parkinson, Scanning tunneling microscopy study of the coverage-dependent structures of pentacene on Au(111), Langmuir **19**, 1274 (2003).

[35] P. G. Schroeder, C. B. France, J. B. Park, and B. A. Parkinson, Energy level alignment and two-dimensional structure of pentacene on Au(111) surfaces, J. Appl. Phys. **91**, 3010 (2002).

[36] S. Lukas, G. Witte, and Ch. Wöll, Novel Mechanism for Molecular Self-Assembly on Metal Substrates: Unidirectional Rows of Pentacene on Cu(110) Produced by a Substrate-Mediated Repulsion, Phys. Rev. Lett. **88**, 028301 (2001).